ELECTRON TRANSPORT PROPERTIES AND DEVICE APPLICATIONS OF NANOCRYSTALLINE SILICON QUANTUM DOTS

H. Mizuta[*1,6], M. Khalafalla[3,6], Z.A.K. Durrani[3,6], S. Uno[4,6], N. Koshida[5,6], Y. Tsuchiya[2,6] and S. Oda[2,6]

[1] Department of Physical Electronics, Tokyo Institute of Technology, Tokyo, Japan

[2] Quantum Nanoelectronics Research Center, Tokyo Institute of Technology, Tokyo, Japan

[3] Microelectronics Research Centre, University of Cambridge, Cambridge, UK

[4] Hitachi Cambridge Laboratory, Hitachi Europe Ltd., Cambridge, UK

[5] Faculty of Technology, Tokyo University of Agriculture and Technology, Tokyo, Japan

[6] CREST, JST (Japan Science and Technology)

ABSTRACT

This paper presents an overview on recent topical studies on electronic properties and device applications of nanocrystalline silicon (nc-Si) quantum dots. We first discuss the electrostatic and quantum-mechanical coherent interactions observed for strongly-coupled double Si nanodots. Secondly we analyze the phononic states and electron-phonon interactions theoretically for the linear chain of Si nanodots covered with thin oxide layers. Finally we discuss a non-volatile nanoelectromechanical memory device which utilizes the single-electron storage of the Si nanodots and the mechanical bistability of a nanoscale freestanding beam.

I. INTRODUCTION

The performance of silicon-based VLSI circuits has steadily been improved over the past decades by scaling down device dimensions, and a nearly exponential growth of microelectronics capabilities has been achieved. However, maintaining this top-down miniaturization trend is getting exceedingly hard due to fundamental physical and technological limitations as well as of the economical limitation although an experimental nanoscale MOSFET with the gate length down to 10 nm has been demonstrated. On the other hand, the use of organic molecules as a building

block for nanoscale devices has attracted much attention since the precisely controlled nanostructures may be formed cheaply by utilizing self-assembly of molecules. This bottom-up technology can potentially overcome the inherent problem of the present silicon top-down technology. The conductivity of the organic molecular structures is, however, still much lower than those for silicon as the electron transport along the single molecule is basically governed by the hopping conduction.

Silicon nanodots and nanorods (see Fig. 1) [1]-[4] may provide a solution to these issues by meeting the requirements both of bottom-up organization and superior carrier transport properties. As those silicon nanostructures can be formed on non-Si substrates such as glass and plastic, the Si-based bottom-up approach may lead to high-performance and large-area electronics. In addition, zero- and one-dimensional nature of electronic states in the individual Si nanodots and nanorods realizes new electronic and photonic properties which are not achieved with bulk silicon. Combining the bottom-up approach with the conventional top-down Si technologies (see Fig. 2) enables us to explore silicon nano-, micro- and macro-electronics on the common technical footing.

This paper focuses on the silicon nanodots and presents recent topical studies on their nanoscale electron transport properties and device applications. For fabricating Si nanodots we have studied three different techniques. The first method is to use a very thin nanocrystalline (nc) Si film with the size of the grains down to a few nanometer. The nc-Si films can be formed either from an amorphous Si film with solid phase crystallization (SPC) or by using a very high frequency (VHF) plasma-enhanced chemical vapour deposition (PECVD) at a low temperature [7]. In the SPC films the individual grains are usually columnar shaped, and the grain boundaries (GBs) between adjacent grains contain carrier trap states due to dangling bonds. On the other hand, in the PECVD films, the individual grains are more spherical, and the GBs are formed by a-Si:H layers between grains. The second approach is to use porous Si [8] formed by using photoanodization of the Si substrate. The surface of the nc-Si islands formed in the substrate can be oxidised selectively by electrochemical oxidation. Formation of a linear chain of nc-Si islands with a diameter as small as 5 nm has been observed [9]. The third approach is a VHF plasma enhanced deposition of silane with a hydrogen gas pulse sequence [10]. This technique facilitates in separating the nucleation and crystal growth process and helps to fabricate nc-Si particles with diameter less than 10 nm and dispersions of 1 nm [11]. Particle diameter down to 3 nm has also been reported recently [12]. The interparticle tunnel barriers can be formed by in-situ oxidation or nitridation in a controlled manner.

In the following sections, we discuss three recent topics on the electron transport properties and device application of the Si nanodots: the electrostatic and quantum-mechanical interactions in double Si nanodots (Section II), the phononic states and electron-phonon interactions in the linear chain of Si nanodots covered with thin oxide layers (Section III), and the non-volatile nanoelectromechanical memory device incorporating Si nanodots (Section IV).

II. INTER-DOT COUPLING EFFECTS IN NC-SI SETs

Nanocrystalline silicon (nc-Si) devices are potential candidates for the development of single-electron transistors (SETs) and quantum information devices compatible with large-scale integration processes. These devices use nanocrystalline silicon materials where nanometre-scale crystalline silicon grains ‘naturally’ form large numbers of silicon quantum dots (QDs), isolated by tunnel barriers formed at thin amorphous silicon or silicon oxide grain boundaries (GBs). The small grain size leads to large electron-confinement and single-electron charging energies, raising the possibility of room-temperature operation of QDs and SETs. The densely-packed nature of the QDs is of also of interest for quantum information processing in silicon.

The close proximity of the nc-Si QDs suggests that strong electrostatic ‘Coulomb’ interactions, and electron wave function interactions, may occur between multiple grains. Electrostatic interactions have been investigated in great detail at milli-Kelvin temperatures in tunnel-coupled double QDs defined in GaAs/AlGaAs two-dimensional electron gas (2-DEG) materials. There are comparatively few investigations of these effects in silicon. These various experiments use two or more gates to change the QD potentials and a plot of the conductance v.s. the two gate voltages traces out hexagonal regions of constant electron number on the QDs, associated with single-electron interactions between the QDs. This forms a ‘charge stability’ diagram where the electron number changes by one between neighbouring hexagons. Electron wave function interactions can also occur, forming coherent ‘quasi-molecular’ states. These states have been observed below 50 mK in conductance measurements on GaAs/AlGaAs double QDs. At the ‘triple-points’ of the charge stability diagram, where two discrete states (one from each QD) are resonant in energy, the inter-dot tunnel coupling forms two ‘valance’ states consisting of bonding-like and anti-bonding-like levels. Resonant tunnelling through these states leads to additional peaks in the device conductance.

We study electrostatic and coherent coupling effects between two adjacent nc-Si grains by using point-contact single-electron transistors (PC-SETs: Fig.3 (left)). The PC-SETs with a very small channel with 30 nm × 30 nm in lateral dimensions were formed on a 40 nm thick nc-Si film with lateral grain size of 20 – 25 nm. The electrostatic potential on the grains are controlled via the bias applied to two side gates. After patterning the PC-SETs, oxidation at 750°C for 60 minutes and annealing at 1000°C were applied, which convert the GBs into a solid tunnel barrier [13]. We observed the switching of the Coulomb oscillation current peaks at 4.2K as we swept the two side gate voltages V_{g1} and V_{g2} (Fig. 3 (right)) [14], and the phenomenon was successfully reproduced using the Monte Carlo single-electron circuit simulation with a model of two parallel, capacitively-coupled Si nanodots (Fig. 4).

Next we adopted oxidation at 750°C for 30 minutes without the following annealing in order for making the GB tunnel barrier more transparent so that the adjacent grains couple each other more tightly. The PC-SETs then exhibited

delocalisation of the electron wavefunctions over the coupled grains. A plot of the device conductance at 4.2 K as a function of the two side gate voltages (Fig. 5(a)) shows single-electron conductance peaks which partially form an electron stability diagram for two charging grains [15]. The peak lines in this plot (white dotted lines) show strong splitting (a dotted circle with 'r') caused by electrostatic interactions when the energy levels in the two grains are in resonance [16]. In this strong coupling region, we observed that the characteristics are decomposed into four Lorentzian peaks (see Figs. 5(b), (c)) – two main peaks with two small peaks. This is attributed to the tunnel coupling across two adjacent Si grains, resulting in bonding- and anti-bonding-like resonance peaks [17]. These molecular states may be used to realize a Si-based charge quantum bit (qubit).

III. PHONONIC BANDGAP IN A SI QUANTUM DOT LINEAR ARRAY

Silicon and its oxides, the key players in the LSIs, now combine in a different way to offer new functional applications in electronics and mechanics. Electron transport properties of the Si nanodots interconnected with thin oxide layers have recently attracted growing attention due to the experimental observation of ballistic electron emission [18]. We investigate the electronic and phononic states in a one-dimensional array of Si nanodots interconnected with thin oxide layers (1DSiNDA) as shown in Fig. 6(a): the individual Si nanodots was simply modeled using a quantum box of 4nm per side sandwiched with 1-nm-thick SiO2 layers. The electron minibands were calculated using the Kronig-Penny potential, and the phonon normal modes were numerically calculated using the atomic linear chain model.

Figure 6(b) shows the phonon dispersion curve and associated phonon density of states (DOSs) calculated for the 1DSiNDA. It can be seen that the spectrum has the energy gaps (phononic bandgaps) and the high-energy optical phonons are virtually dispersionless, which indicates the optical phonons are confined in the Si dots. Consequently, the electron-phonon interactions differ significantly from those for bulk Si: the acoustic phonon scattering potential is reduced and the inter-miniband scattering is prohibited as the electronic miniband gaps are larger than the maximum available phonon energy. These phenomena may lead to less electron energy dissipation in the system.

The electron-phonon scattering potential for the 1DSiNDA is expressed as $H_{el-ph}(x) = D_{aco}\,\partial S(x)/\partial x$ where $S(x)$ and D_{aco} denote phonon wave function and the coupling constant, respectively. The first derivative of $S(x)$ is also known as the strain. Figure 7 compares the strain in the 1DSiNDA (a thin solid line with open circles) and conventional Si quantum wire (a broken line). Note that the oxide layers 'absorb' the strain from the Si nanodots [19]. This is reasonable because the oxide

layers are ‘softer’ than Si nanodots (the Young’s modulus of Si and oxide are 180GPa and 70GPa, respectively). As the coupling constant D_{aco} in the oxide is smaller than that in Si, the strain absorption effect reduces the scattering potential over the entire region in 1DSiNDA compared to that of Si quantum wire. This may lead to a significant reduction of electron-phonon scattering.

We also found that the associated electron energy loss is suppressed in the 1DSiNDA [19]. Figure 8 shows the electron energy loss per unit time caused by the phonon scattering in the 1DSiNDA, calculated for an electron miniband. Note that the energy loss rate is significantly suppressed at the vicinity of the miniband bottom energy. Thus, the electron energy loss becomes much less than that in the Si nanowires. These results indicate that the phonon dispersion and the associated electron-phonon interactions may be tuned to decrease the electron energy loss in the Si nanodot cluster.

IV. SI NANODOT NONVOLATILE NANOELECTROMECHANICAL MEMORY

Silicon-based nano Electro-Mechanical Systems (NEMS) have recently been of great interest from stand-points of their extremely high-speed operation [21] as well as physics of electron transport coupled with a nanoscale mechanical resonator [22][23]. We recently proposed a new nonvolatile memory concept based on bistable operation of the NEMS structure combined with the Si nanodots (Fig.9) [24][25]. Our NEMS memory features a beam suspended in the cavity placed under the gate electrode, which contains the Si nanodots as charge storage. The beam acts as a floating gate of the memory with being bent either upward or downward. When the gate voltage is applied, the floating gate beam moves via electrostatic interactions between the gate electrode and the charge in the Si nanodots. The switching speed between two stable states was estimated to be ~ 0.5 ns for a SiO_2 beam with the dimension of 1.0 × 1.0 × 0.1 μm^3, from a mechanical analysis assuming the maximum central displacement of 35 nm.

A positional displacement of the floating gate may be sensed with a change in the drain current of the MOSFET underneath. Mechanical bistablity of the beam is therefore essential for achieving our non-volatile NEMS memory, and a higher switching speed is expected with reducing their dimensions down to the nanometer regime. As the switching mechanism does not depend on any charge tunneling through the gate oxide, we may avoid the gate oxide degradation, which is one of the serious issues in the conventional flash memory.

Mechanical properties of the beam were analyzed by using a parallel three-dimensional (3D) finite element simulation. A nc-Si beam structure, in which a two-dimensional array of Si nanodots are embedded in a SiO_2 film (Fig. 10(a)), was compared with a simple poly-Si beam structure, in which a thin Si sheet are placed between SiO_2 layers. The Young’s modulus and Poisson’s ratio of 190 GPa and 0.27 for Si, and 70 GPa and 0.175 for SiO_2 were used for the present simulation. Calculated 3D images of the beam deformed under a constant homogeneous pressure

parallel to Z-axis are shown in Fig. 10(b). The maximum central displacement obtained for the nc-Si beam was found larger than that for the poly-Si beam with the same pressure. This indicates that a larger displacement is achievable for the nc-Si beam structure under the same external electric filed and, therefore, the nc-Si beam has an advantage for low power operation.

In order for investigating the mechanical properties of beam structure experimentally, the nano-indentor type loading system [26] was used. For this experiment, a single layer SiO_2 beam structure was fabricated using a dry etching Si undercut technique. The most of the fabricated samples showed an upward bent beam as shown in Fig. 11(a), and this is considered as a result of release of mechanical stress stored in SiO_2 after removing a Si layer underneath. However, few samples showed a downward bent beam (Fig. 11(b)), and this fact indicates that the beam has a mechanically bistable states. We loaded the upward bent beam with the tip of the nano-indentor around the center of the beam. After the loading we observed that the beam was switched to the downward bend position, and this confirms that the bistable states can be switched by applying an external force.

V. SUMMARY

We presented recent studies on electronic properties and device applications of the nc-Si quantum dots. We first discussed the electrostatic and coherent coupling of electronic states in double Si nanodots interacting each other. Single-electron conductance peaks are seen at 4.2 K as a function of two gate voltages, caused by electrostatic coupling between the Si nanodots. Additional conductance peaks are observed when the energy levels from two adjacent nanodots are resonant. These peaks may be associated with ‘quasi-molecular’ states formed by coherent coupling of the energy levels in the nanodots. Secondly, we theoretically studied electronic and phononic states in the 1D silicon/oxide heterostructure. The results showed that the phonon emission rate is larger than the one calculated for Si quantum wire, while the energy loss rates at near the bottom of minibands are much smaller, showing energy ranges at which energy loss is strongly suppressed. Thirdly, we investigated a new non-volatile NEMS memory device with the Si nanodots embedded in a movable floating gate beam. Advantage of using the Si nanodots array for the movable floating gate beam was shown for low power operation. The mechanical bistability of the fabricated SiO_2 beam was clearly observed.

ACKNOWLEDGMENT

The authors are very grateful to Mr. K. Takai, Mr. N. Momo, Mr. K. Usami, Mr. S. Higashijima, Mr. Y. Kurokawa of Tokyo Institute of Technology for their valuable technical contributions, and Dr. T. Shimada, Dr S. Yamaguchi, Dr. S. Saito, Dr. Arai of Central Research Laboratory, Hitachi Ltd., Prof. K. Nakazato of Nagoya University, Prof. N. Mori of Osaka University, Dr. T. A. Armour of Nottingham University for very useful discussions.

References

[1] Y. Cui and C. M. Lieber., Science 291, 851 (2001)
[2] Y. Huang, X. Duan, Q. Wei, C. M. Lieber, Science 291, 630 (2001)
[3] X. Duan, C. Niu, V. Sahi, J. Chen, J.W. Parce, S. Empedocles and J.L. Goldman, Nature 425, 274 (2003)
[4] S. Piscanec, M. Cantoro, A.C. Ferrari, J.A. Zapien, Y. Lifshitz, S.T. Lee, S. Hofmann and J. Robertson, Phys. Rev. B68, 241312 (2003)
[5] P. Ordejon, E. Artacho and J. M. Soler, Phys. Rev. B (Rapid Comm.) 53, R10441 (1996)
[6] J. M. Soler, E. Artacho, J.D. Gale, A. Garcia, J. Junquera, P. Ordejon and D. Sanchez-Portal, J. Phys.: Condens. Matt. 14, 2745 (2002)
[7] T. Kamiya, K. Nakahata, Y. T. Tan, Z.A.K Durrani and I. Shimizu, J. Appl. Phys. 89, 6265 (2001)
[8] N. Koshida and H. Koyama, Appl. Phys. Lett. 60, 347 (1992)
[9] A.G. Cullis, L.T. Canham and P.D.J. Calcott,, J. Appl. Phys. 82, 909 (1997)
[10] S. Oda and M. Otabe, Mater. Res. Soc. Proc. 358, 721 (1995)
[11] T. Ifuku, M. Otabe, A. Itoh and S. Oda, Jpn. J. Appl. Phys. 36, 4031 (1997)
[12] J. De Blauwe, *et al*., *IEDM Tech. Dig.*, 683 (2000)
[13] Y. T. Tan, T. Kamiya, Z. A. K. Durrani, and H. Ahmed, J. Appl. Phys. 94, 633 (2003)
[14] M. Khalafalla, H. Mizuta, and Z. A. K. Durrani, IEEE Trans. Nanotechnol. 2, 271 (2003).
[15] W. G. van der Wiel, S. De Franceschi, J. M. Elzerman, L. P. Kouwenhoven, T. Fujisawa, and S. Tarucha, Rev. Mod. Phys. 75, 1 (2003).
[16] M. Khalafalla, H. Mizuta, and Z. A. K. Durrani, in press for Appl. Phys. Lett. (2004)
[17] R. H. Blick, D. Pfannkuche, R. J. Haug, K.v. Klitzing, and K. Eberl, Phys. Rev. Lett. 80, 4032 (1998).
[18] N. Koshida, X. Sheng and T. Komoda, Appl. Surf. Sci., 146, 371 (1999).
[19] S. Uno, K. Nakazato, S. Yamaguchi, A. Kojima, N. Kojima and H. Mizuta, IEEE Trans. Nanotechnol. 2, 301 (2003)
[20] S. Uno, N. Mori, K. Nakazato, N. Koshida and H. Mizuta, Silicon Nanoelectronics Workshop, Honolulu, (2004)
[21] X.M.H. Huang, C. A. Zorman, M. Mehregany, M. L. Roukes, Nature 421, 496 (2003).
[22] E. M. Weig, R. H. Blick, T. Brandes, J. Kirschbaum, W.Wegscheider, M. Bichler and J. P. Kotthaus, Phys. Rev. Letts. 92, 046804 (2004)
[23] A. D. Armour, M. P. Blencowe and Y. Zhang, Phys. Rev. B69, 125313 (2004)
[24] Y. Tsuchiya, K. Takai, N. Momo, S. Yamaguchi, T. Shimada, S. Koyama, K. Takashima, Y. Higo, H. Mizuta and S. Oda, Silicon Nanoelectronics Workshop, Honolulu (2004)
[25] Y. Tsuchiya, K. Takai, N. Momo, S. Oda, S. Yamaguchi, T. Shimada and H. Mizuta, 27th International Conference on the Physics of Semiconductors (ICPS27), Flagstaff (2004).
[26] K. Takashim, Y. Higo, S. Sugiura and M. Shimojo, Mat. Trans. 42, 68 (2001)

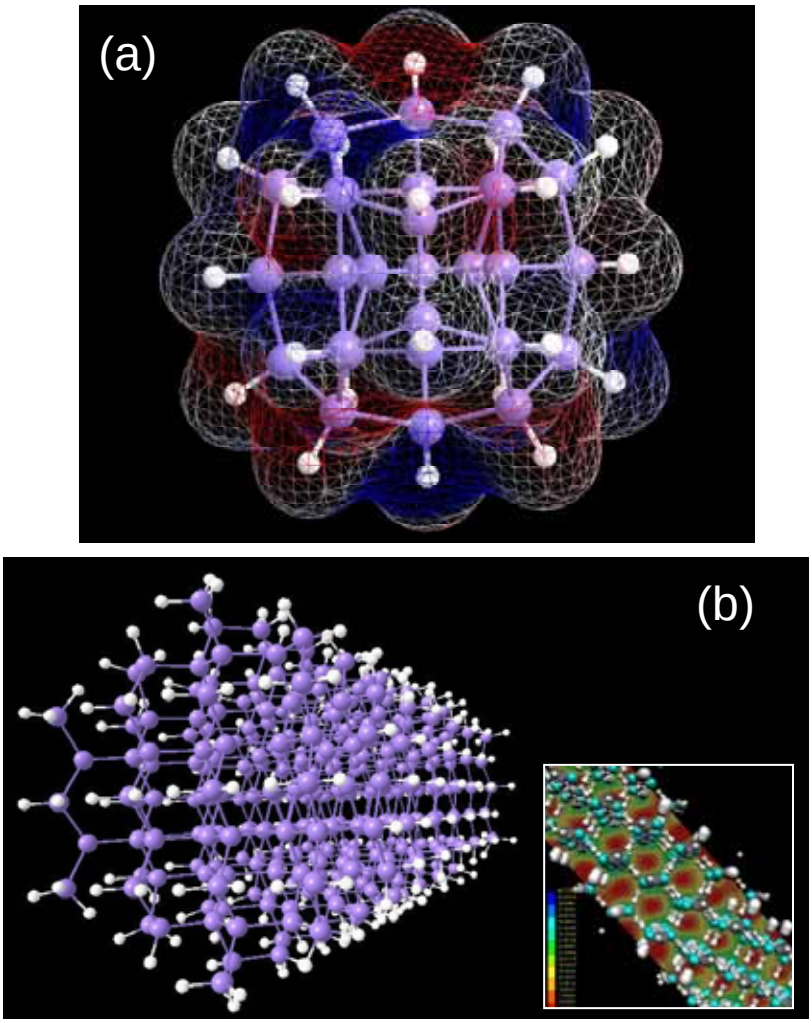

Figure 1: Atomic structures of (a) a hydrogen-terminated silicon nanodot ($Si_{29}H_{24}$) with diameter of 1 nm and (b) a hydrogen-terminated silicon nanorod ($Si_{336}H_{250}$) with diameter of 1 nm and length of 3 nm calculated using the *ab-initio* DFT simulation SIESTA [5][6].

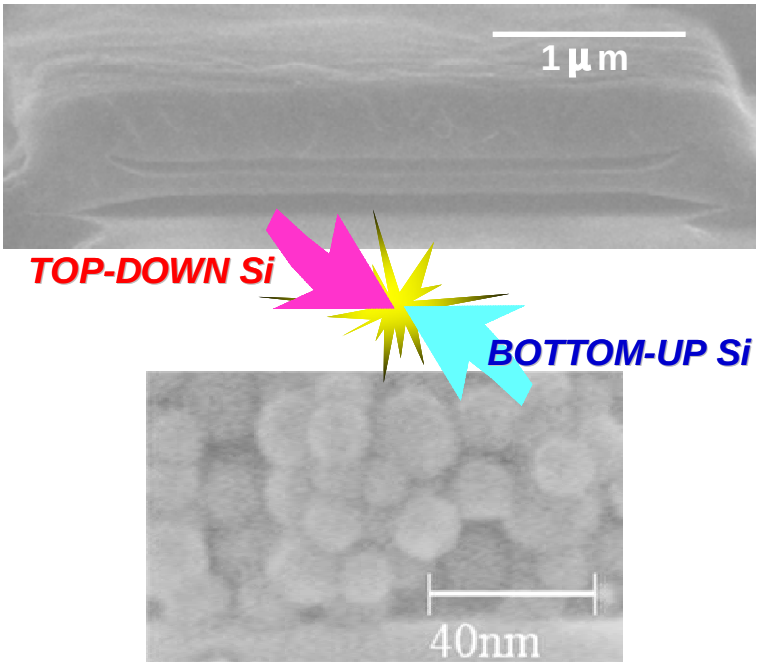

Figure 2: Combination of top-down (nanolithography) and bottom-up (assembly of nanoscale building blocks) approaches opens a new pathway for fabricating silicon nanoelectronic devices.

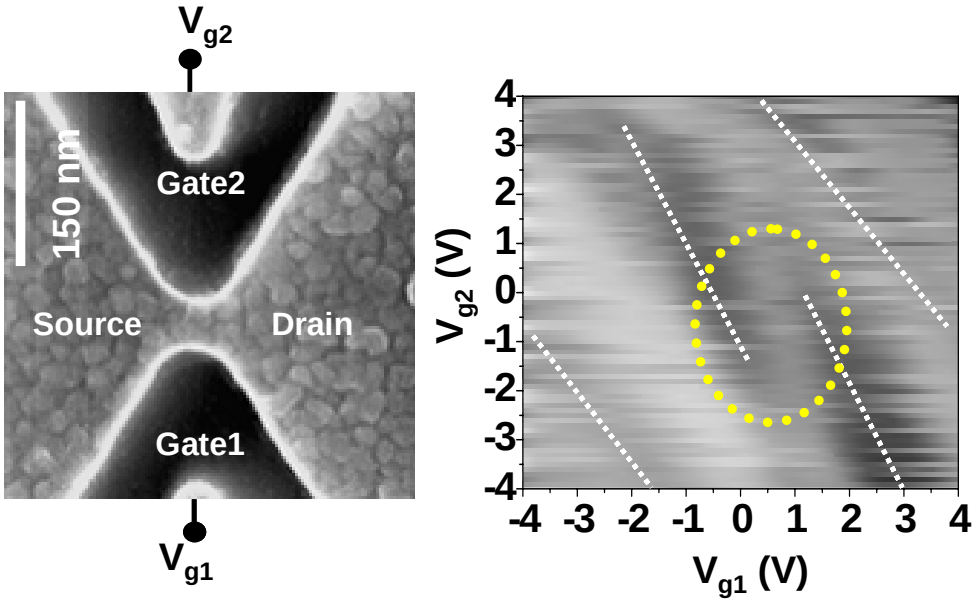

Figure 3: A SEM micrograph of a nano-Si point contact transistor (left) and gray scale image of current as a function of two side gate bias voltages V_{g1} and V_{g2} (right). A thick dotted circle indicates the switching region of the peak current line.

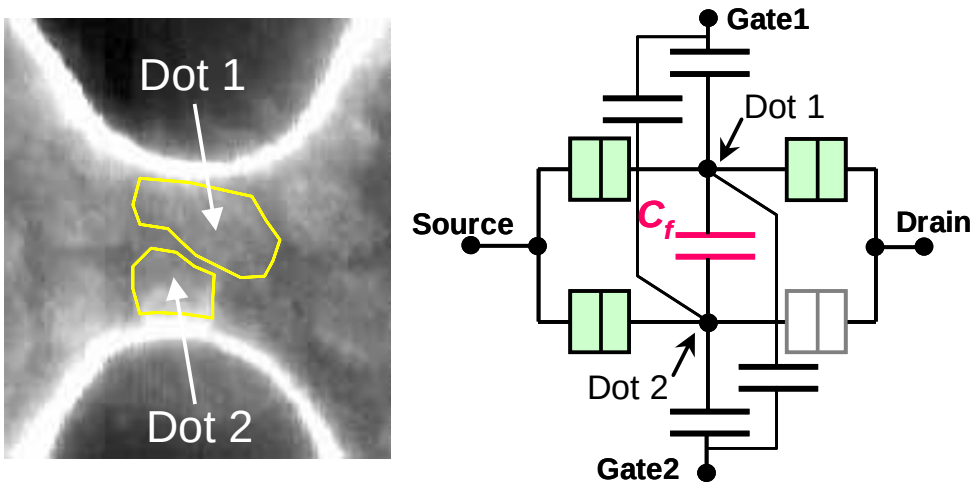

Figure 4: A blow-up of the point-contact channel with two Si grains, Dot 1 and Dot 2, indicated by thin lines (left) and an equivalent circuit for the capacitively coupled double parallel quantum dots dots (right)

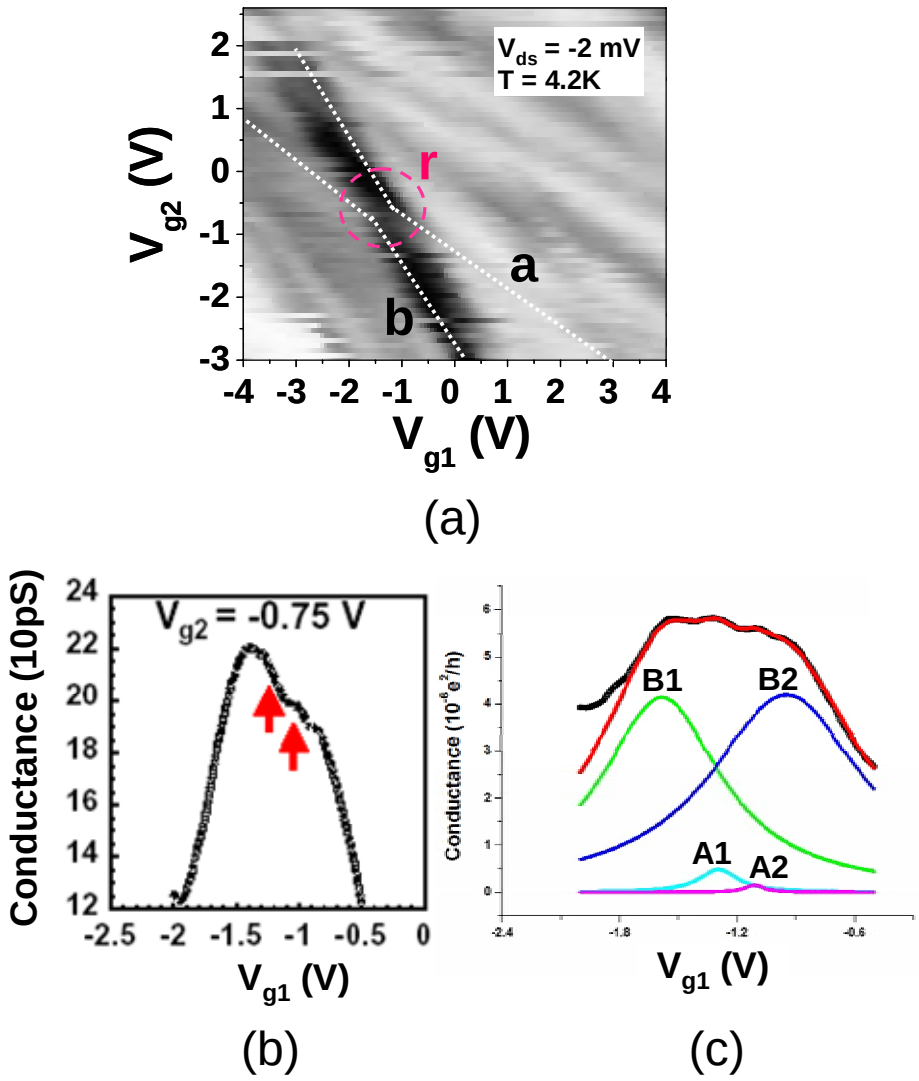

Figure 5: (a) A gray scale image of current as a function of two side gate bias voltages V_{g1} and V_{g2} for the PC-SET with tunnel-coupled double Si nanodots. (b) A fine current structure observed around the triple points (shown by a broken circle with 'r' in (a)) and (c) its decomposition into four Lorenzian peaks.

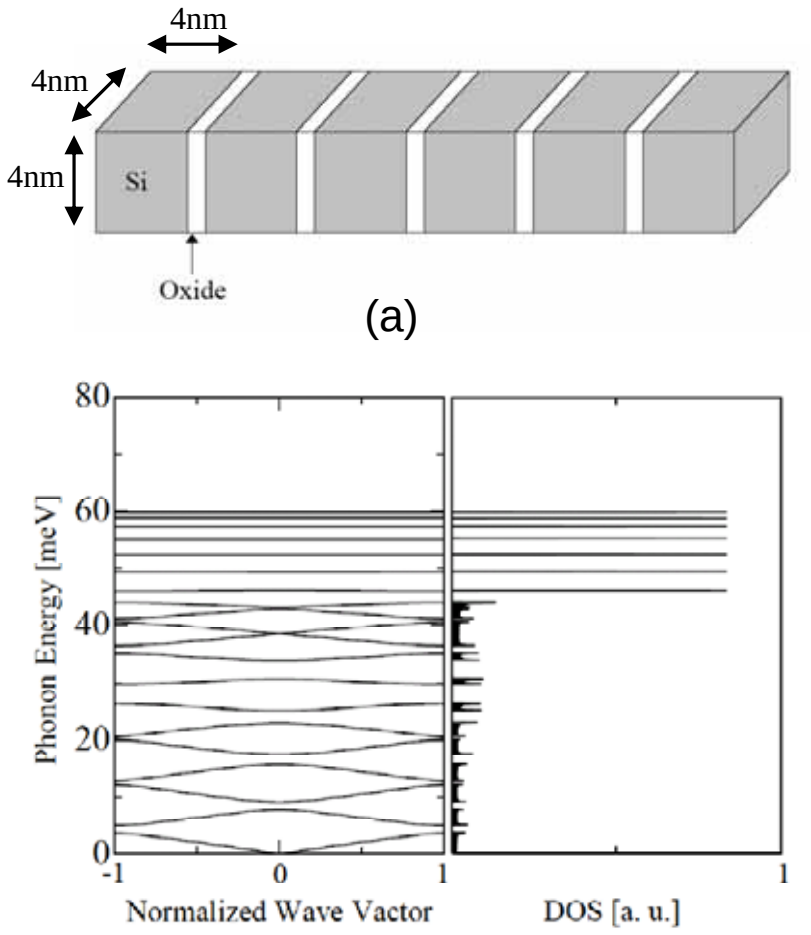

Figure 6: (a) Schematic illustration of the1DSiNDA structure used for the calculations and (b) the calculated phonon energy dispersion (left) and the associated density of state (DOS).

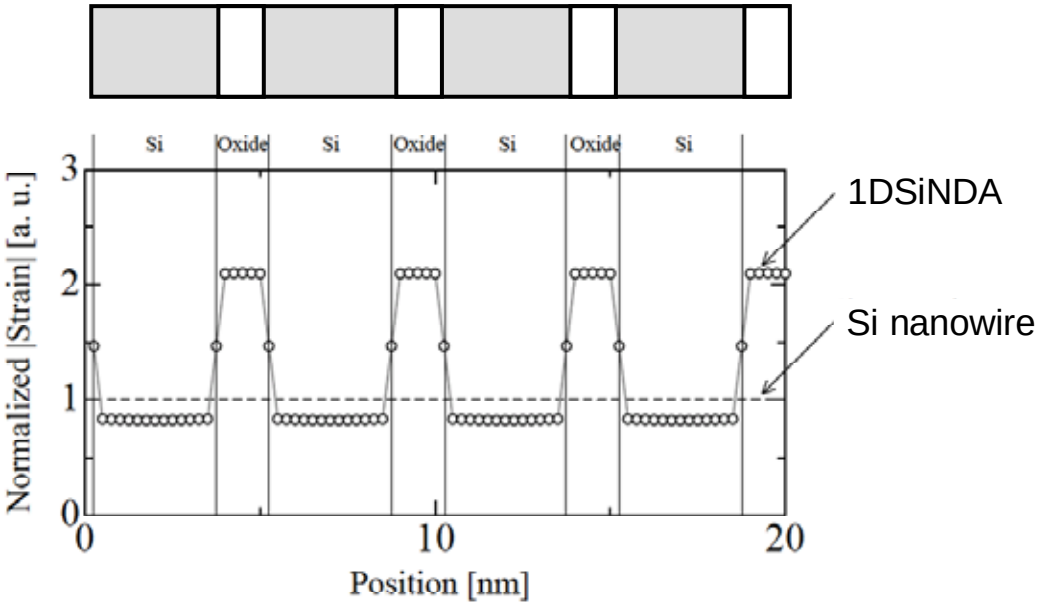

Figure 7: Spatial distribution of strain caused by the phonon calculated for the 1DSiNDA (a solid line with open circles) and a simple Si nanowire (a broken line).

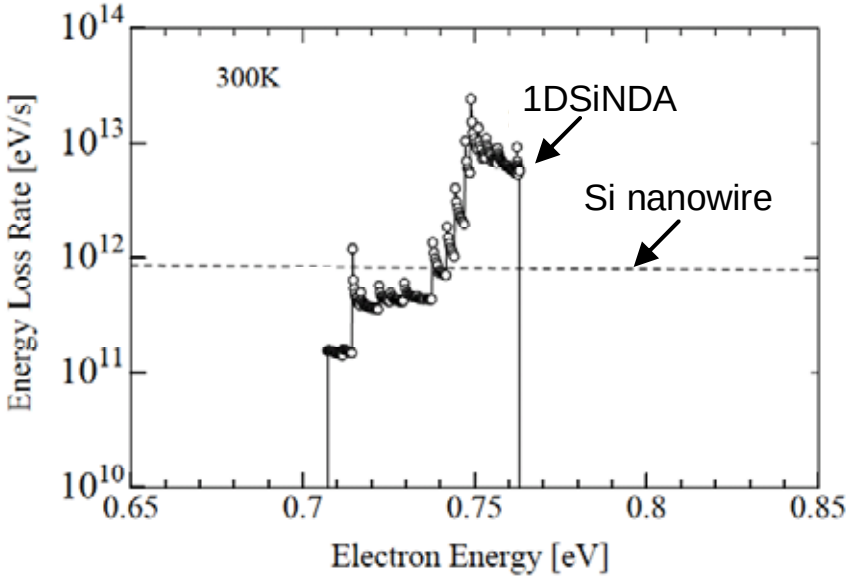

Figure 8: Energy loss rate as a function of electron energy calculated for the 1DSiNDA (a solid line with open circles) and Si nanowire (a broken line).

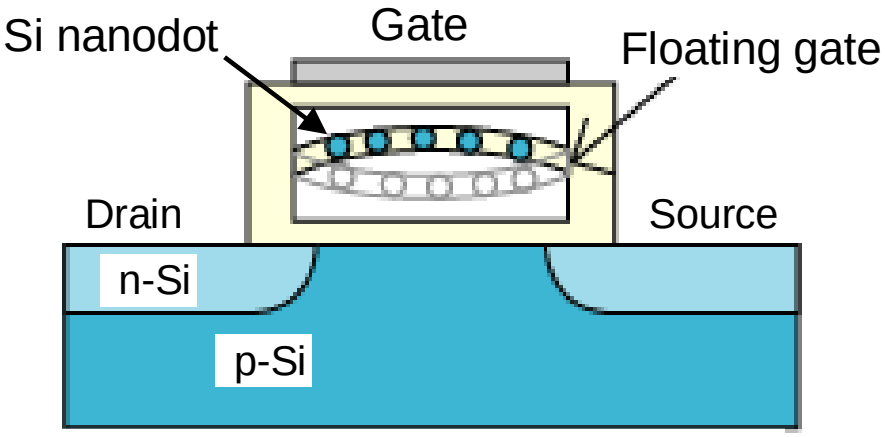

Figure 9: A schematic cross-sectional view of a NEMS memory device which operates based on mechanical flip-flop motion of the thin beam incorporating the nc-Si quantum dots.

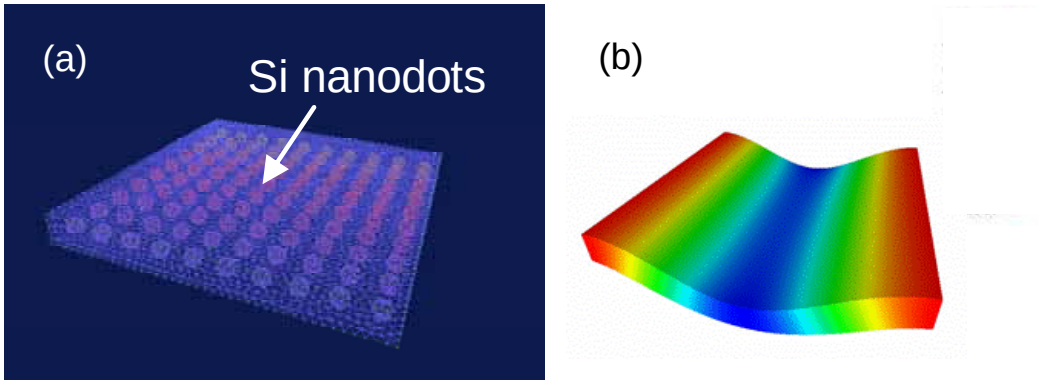

Figure 10: (a) A SiO_2 beam incorporating Si nanodots used for 3D FE simulation and (b) the beam deformed downward under a uniaxial force applied perpendicular to the beam.

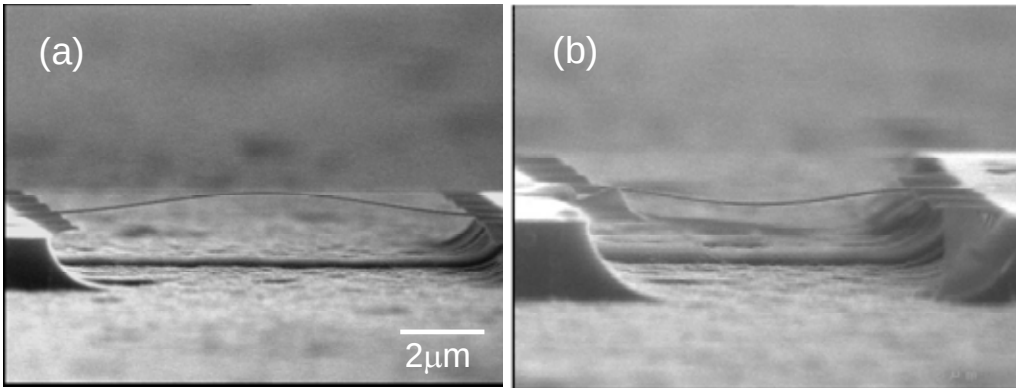

Figure 11: A mechanically-bistable free standing SiO_2 beam: observed two stable forms, bent (a) upward and (b) downward.